Structure, Luminescence, and Dynamics of Eu_2O_3 Nanoparticles in MCM-41

Wei Chen,*,† Alan G. Joly,‡ Collin M. Kowalchuk,§ Jan-Olle Malm,|| Yining Huang,§ and Jan-Olov Bovin||

Nomadics, Inc., 1024 South Innovation Way, Stillwater, Oklahoma 74074, Pacific Northwest National Laboratory, P.O. Box 999, Richland, Washington 99352, Department of Chemistry, University of Western Ontario, London, Ontario, Canada N6A 5B7, and Materials Chemistry, Center for Chemistry and Chemical Engineering, Lund University, P.O. Box 124, SE-22100, Lund, Sweden

Received: March 22, 2002

The structure, luminescence spectroscopy, and lifetime decay dynamics of Eu_2O_3 nanoparticles formed in MCM-41 have been investigated. Both X-ray diffraction and high-resolution transmission electron microscopic observations indicate that Eu_2O_3 nanoparticles of monoclinic structure are formed inside channels of MCM-41 by heating at 140 °C. However, heat treatment at 600 or 700 °C causes migration of Eu_2O_3 from the MCM-41 channels, forming nanoparticles of cubic structure outside the MCM-41 channels. After heating to 900 °C, some of the cubic Eu_2O_3 particles change to monoclinic Eu_2O_3, and the MCM-41 structure breaks down and a different or disordered phase is formed. The feature of the hypersensitive $^5D_0 \rightarrow {}^7F_2$ emission profile of Eu^{3+} is used to follow the structural changes. In the luminescence spectrum of the sample prepared at 140 °C, the emission spectrum is dominated by peaks at 615 and 623 nm, while in the other samples a peak at 612 nm is prevalent. Photoluminescence lifetimes show the existence of short (<1 μs) and long (microsecond to millisecond) components for each sample. The fast decay is attributed to quenching by surface states of the nanoparticles or energy transfer to the MCM-41, while the longer time decays show the effects of concentration quenching. The monoclinic sample prepared at 140 °C shows a higher luminescence intensity than the cubic samples or the bulk powder. These observations indicate that MCM-41 as a template can be used for making and stabilizing monoclinic rare earth oxides, which normally are stable only at high temperatures and high pressures. More importantly, the nanophase Eu_2O_3/MCM-41 composite materials formed at low temperatures might represent a new type of efficient luminescence material with fast response, with potential applications in lighting and displays.

1. Introduction

The unique physical and chemical properties of the lanthanide oxides make them useful in a variety of diverse applications, such as laser materials,[1] phosphors,[2] and heterogeneous chemical catalysis.[3] The luminescence of Eu^{3+} is particularly interesting because the major emission band is centered near 612 nm (red), which is one of the three primary colors (red, blue, and green) from which a wide spectrum of colors, including white, can be generated by appropriate mixing. For this reason, Eu^{3+} has been thoroughly investigated as a luminescent activator in many host lattices.[4,5] Indeed, Eu^{3+} doped in Y_2O_3 is a commercially available phosphor with extremely high quantum efficiency. In several aspects, oxide phosphors may be better suited than sulfides for applications such as low-voltage cathodoluminescent devices, primarily because oxide phosphors show improved stability in high-vacuum environments as well as lower contaminant gas emission.[3] Eu_2O_3 is one of the most important oxide phosphors and has been studied extensively.[2,3,6,7]

Due to quantum confinement, a large ratio of surface to volume, and the geometrical confinement of phonons, semiconductor nanoparticles behave differently from bulk materials and have some novel properties and effects. More and more evidence has emerged showing that quantum size confinement not only affects the intrinsic properties of semiconductors but also changes the properties of doped ions.[8−11] The spectroscopic properties of Eu_2O_3 nanoparticles prepared by laser evaporation,[12−16] sol−gel,[17] and colloidal chemistry[18] have been reported. Electron−phonon interaction and spectral hole-burning have been reported in Eu_2O_3 nanoparticles.[19,20] All these studies have demonstrated some novel properties and potential applications of Eu_2O_3 nanoparticles. Furthermore, the luminescence time dependence of Eu_2O_3 nanoparticles deposited on and doped in alumina has been investigated.[21] The coated samples show a short, 340 μs lifetime, while the Eu^{3+} doped in the alumina display a much longer, 1.5 ms lifetime.[21] This difference was attributed to a reduction in concentration quenching in the doped sample.[21] An increase in the decay lifetime of Eu^{3+} in Y_2O_3[12,16] and Eu_2O_3[14] nanoparticles with decreasing size has been reported by Tissue and Bihari[15] and has been attributed to a decrease in the radiative decay rate with decreasing size. To further reveal the effect of quantum size confinement on the luminescence decay of Eu_2O_3 nanoparticles, we describe the effect of size confinement on the structure, luminescence, and decay dynamics of Eu_2O_3 nanoparticles formed in the mesoporous silicate MCM-41.

2. Experimental Details

MCM-41 was prepared under hydrothermal conditions by literature procedures.[22,23] N-Brand sodium silicate (18.7 g) was

* Corresponding author: e-mail wchen@nomadics.com.
† Nomadics, Inc.
‡ Pacific Northwest National Laboratory.
§ University of Western Ontario.
|| Lund University.

10.1021/jp020787a CCC: $22.00
Published on Web 06/20/2002

combined with H_2O (40.0 g, 2.22 mol) and H_2SO_4 (1.20 g, 12.2 mmol). The solution was stirred for 10 min to obtain a homogeneous white solution. The template C16-TMA-Br (16.8 g, 46.1 mmol) was added to the solution with additional H_2O (55.0 g, 3.06 mol), and the mixture was stirred for 0.5 h. Further H_2O (15.5 g, 0.861 mol) was added and the solution was transferred to a stainless steel bomb and heated at 100 °C for 165 h. The resulting white powder was calcined at 540 °C for 10 h to remove the organic template. Identity of the product was confirmed by powder X-ray diffraction (XRD) and nitrogen adsorption. From the XRD study it was observed that MCM-41 had the characteristic diffraction pattern (h_{100}, h_{110}, h_{200}) indexed from a hexagonal cell.[22] The *d* spacings are 3.83 nm (d_{100}), 2.22 nm (d_{110}), and 1.96 nm (d_{200}). It is possible to calculate the pore diameter from the d_{100} spacing. A value of 4.42 nm is obtained, and subtracting 1 nm resulting from the average diameter of the pore wall provides a channel diameter of 3.42 nm. The nitrogen adsorption isotherm has a Brunauer−Emmett−Teller (BET) surface area of 1172 m^2/g resulting from a characteristic type IV isotherm and distinct capillary condensation.[23] The pore diameter is confirmed with a value of 3.5 nm calculated from 4 V/A (by BET), which compares closely to the value obtained by XRD.

The formation of Eu_2O_3 nanoparticles in the channels of MCM-41 was conducted at high temperatures by solid-state diffusion. Typically, 1 g of MCM-41 powder was mixed with 0.005 g of Eu_2O_3 powder in an ethanol solution. After drying at room temperature, the mixed powder was heated at 140, 600, 700, or 900 °C for 3 h. The particle structure, size, and stability were studied by X-ray diffraction, analytical and high-resolution transmission electron microscopy (HRTEM). The X-ray diffraction patterns were recorded with a Rigaku diffractometer with graphite-monochromated Co Kα radiation of wavelength 0.179 02 nm. Thin fragments of the samples were collected on lacy carbon film on copper grids for analytical electron microscopy. HRTEM images of the sample prepared at 700 °C particles were recorded with a JEM-4000EX operated at 400 kV and with a structural resolution of 0.16 nm. Energy-dispersive X-ray analysis (EDX) was performed with a JEM-2000FX using a LINK spectrometer. Electron energy loss spectroscopy (EELS) was performed with a GIF 100 mounted on a Philips CM120 microscope. Energy-selected elemental mapping was done for silicon (Si-$L_{2,3}$ edge at 99 eV) and for europium (Eu-$N_{4,5}$ edge at 130 eV) on the two samples prepared at 140 and 700 °C. The Si-$L_{2,3}$ edge has a delayed edge with a maximum at about 130 eV and consequently the three-window method of elemental mapping for the Eu edge must be performed with very narrow energy windows (5 eV).

The photoluminescence (PL) emission spectra were recorded at room temperature on a Spex Fluorolog fluorescence spectrophotometer. The time-resolved spectra and luminescence lifetime data were collected with a nanosecond optical parametric oscillator/amplifer (OPO) operating at a 10 Hz repetition rate and tunable between 440 and 1800 nm. The output was directed onto the particles and emission was collected at right angles to the excitation and focused into a 1/8 m monochromator with a standard photomultiplier tube detector (used for lifetime measurements) or a gated intensified charge-coupled device (CCD) camera (used for spectra). The output of the photomultiplier tube was directed into a digital oscilloscope to record the emission decays. The response time of the system is about 15 ns fwhm. Picosecond lifetime data was collected by using the output of a femtosecond-amplified Ti:sapphire laser operating at 1 kHz. The 150 fs, 800 nm output was frequency-doubled in a 1 mm Beta Barium Borate crystal to provide excitation at 400 nm and directed onto the samples. The output emission was collected at right angles and focused into the entrance of a streak camera (Hamamatsu C5680). Appropriate filters were used to isolate the wavelengths of interest. The time resolution was determined to be 14 ps fwhm by use of a standard scattering material.

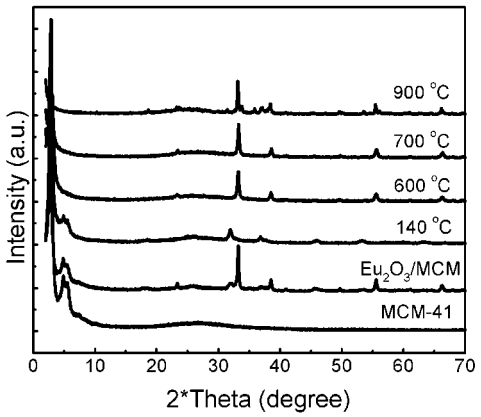

Figure 1. XRD patterns of MCM-41, a Eu_2O_3/MCM-41 mixture, and the samples prepared by heat treatment at 140, 600, 700, and 900 °C.

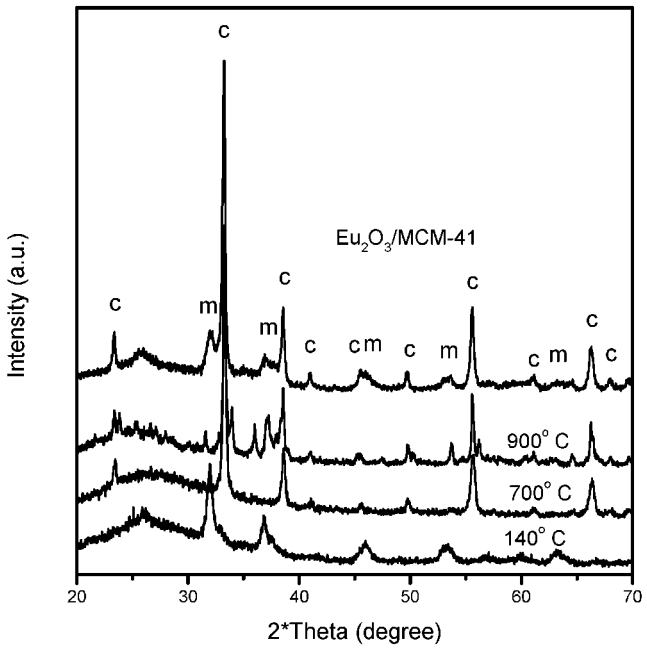

Figure 2. Enlarged XRD patterns of the Eu_2O_3/MCM-41 mixture, and the samples prepared by heat treatment at 140, 600, 700, and 900 °C (c = cubic, m = monoclinic).

3. Results

Figures 1−3 show the XRD patterns of MCM-41, a Eu_2O_3/MCM-41 mixture, and the samples prepared by heat treatment at 140, 600, 700, and 900 °C. The Eu_2O_3 source has two phases, cubic and monoclinic, which are labeled in the pattern. It is interesting to note that, after heat treatment at 140 °C, a pure monoclinic Eu_2O_3 is observed. After heat treatment at 600 or 700 °C, the Eu_2O_3 changes to a cubic structure. Heat treatment at 900 °C results in both cubic and monoclinic phases (Figure 2).

The above phase changes during heat treatment at different temperatures are confirmed by the particle sizes estimated from XRD and HRTEM observations. As a result of size and/or strain,

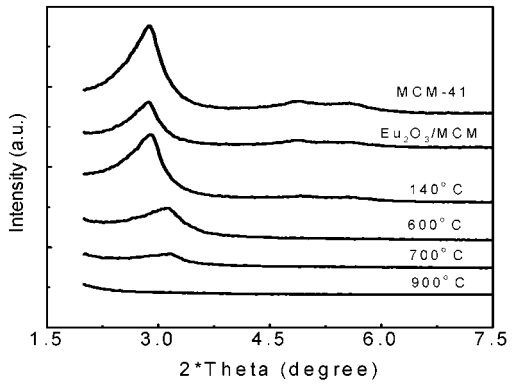

Figure 3. Enlarged XRD patterns of MCM-41, the Eu_2O_3/MCM-41 mixture, and the samples prepared by heat treatment at 140, 600, 700, and 900 °C.

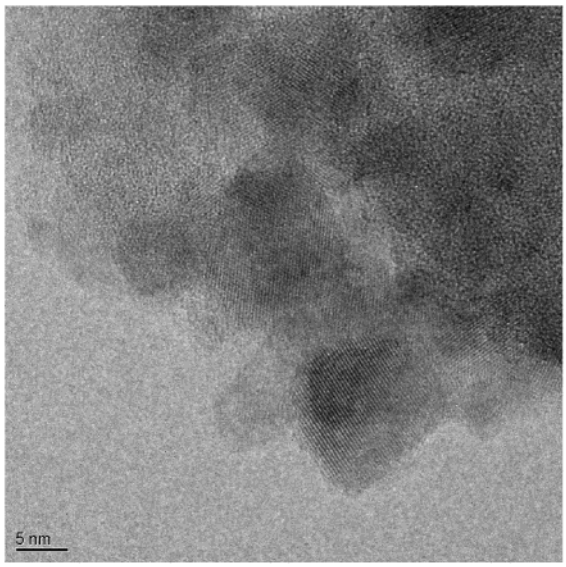

Figure 4. Fragments of Eu_2O_3/MCM-41 prepared at 700 °C show a lattice spacing of 1 nm when imaged by HRTEM.

the XRD peaks are broadened.[24] From the Debye−Scherrer equation,[24] the average sizes of the nanoparticles can be approximated from the XRD peak half-width by assuming that there is no strain. For the sample prepared at 140 °C, the particle size is around 3 nm, which is close to the cavity diameter (3.5 nm) of MCM-41, allowing the particles to be formed within the hexagonal channels. At 600 and 700 °C, the particle sizes are around 5 and 7 nm, respectively. At 900 °C, the size of the cubic Eu_2O_3 is about 10 nm and the monoclinic phase is about 4 nm in size. After heat treatment at 600, 700, or 900 °C, the particle sizes are larger than the cavity diameter of MCM-41. This indicates that Eu_2O_3 is formed outside the cavities of MCM-41. Heating at 900 °C produces both cubic and monoclinic Eu_2O_3, and the XRD peaks of MCM-41 disappear. This indicates that MCM-41 breaks down at 900 °C and most likely becomes a different or disordered phase of SiO_2.

To confirm the above observations from XRD studies, we have used HRTEM to image the samples prepared at 700 °C. Figure 4 shows a HRTEM image of Eu_2O_3/MCM-41 prepared at 700 °C. The Eu_2O_3 particles imaged by HRTEM have an average size of about 8 nm. The (100) lattice spacing in some of the particles was estimated to be about 1 nm. This is close to the lattice spacing of cubic Eu_2O_3 ($a = 1.087$ nm). These observations are in agreement with the conclusion from the XRD studies.

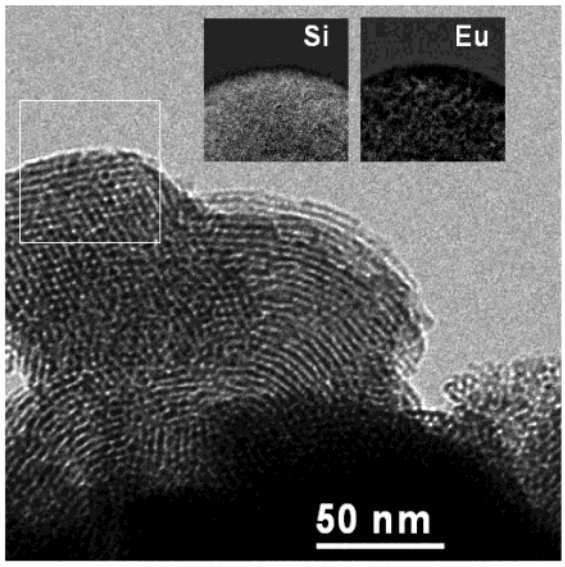

Figure 5. Energy-selected imaging (main picture) of MCM-41 fragments and three- window elemental mapping (inserted maps) of silicon and europium reveal the existence of Si and Eu in the same region in the sample prepared at 700 °C.

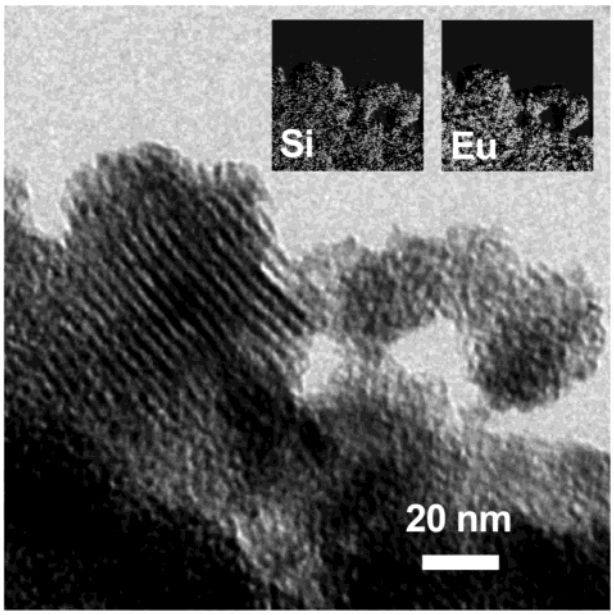

Figure 6. Energy-selected imaging (main picture) of MCM-41 fragments and three- window elemental mapping (inserted maps) of silicon and europium reveal the existence of Si and Eu in the same region in the sample prepared at 140 °C.

Analytical electron microscopy using energy-dispersive spectrometry (EDS) and elemental mapping shows that europium exist either outside or inside the MCM-41 particles. Three-window elemental mapping also shows that europium exists in the same region as the silicon of the MCM-41 particles (see Figure 5). These analytical TEM methods however, do not prove that europium fills the channels of MCM-41 in this sample. A similar result is observed for the sample prepared at 140 °C (Figure 6). In this sample, with the electron beam focused on the edge of MCM-41 fragments, the EDS spectra indicate small levels of Eu. The mapping results cannot show clearly that Eu_2O_3 particles are inside or outside the channels of MCM-41. This is probably because the mapping resolution is not good enough. However, the combination of XRD, HRTEM, mapping,

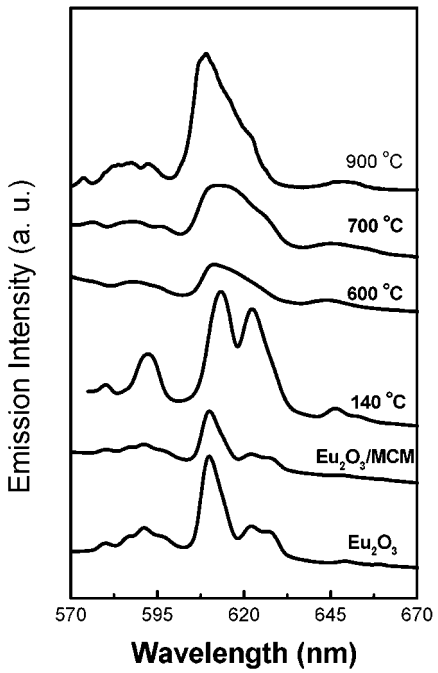

Figure 7. Luminescence spectra (excitation at 393 nm) of Eu_2O_3, a Eu_2O_3/MCM-41 mixture, and the samples prepared by heat treatment at 140, 600, 700, and 900 °C.

and luminescence properties provides strong evidence for the formation of Eu_2O_3 nanoparticles in MCM-41.

The formation and structures of Eu_2O_3 nanoparticles in MCM-41 can be further confirmed by the luminescence characteristics of Eu^{3+}. In monoclinic and cubic Eu_2O_3, the emission spectra of Eu^{3+} are different in both relative intensities and positions because the effects of the crystal field perturbations on the individual f−f transitions are different. The $^5D_0 \rightarrow {}^7F_2$ transition is highly sensitive to structural change and environmental effects;[25] therefore, this transition can be used for distinguishing the two structures.[26] It has been shown that, upon the change from cubic to monoclinic Eu_2O_3, the $^5D_0 \rightarrow {}^7F_2$ emission peak at 612 nm decreases in intensity or disappears, while the $^5D_0 \rightarrow {}^7F_2$ emission peak between 620 and 630 nm appears or increases in intensity.[26] In addition, peaks at 614 and 618 nm may appear in the monoclinic phase.[13−15] Figure 7 shows the luminescence spectra of Eu_2O_3, a Eu_2O_3/MCM-41 mixture, and the samples prepared by heat treatment at 140, 600, 700, and 900 °C. The primary peak centered around 612 nm and extending to 620 nm is the $^5D_0 \rightarrow {}^7F_2$ transition. The $^5D_0 \rightarrow {}^7F_2$ is composed of several subbands, which are split by crystal field perturbations.[25] The emission spectrum of the sample prepared at 140 °C is significantly different from those of the other samples. In this sample, the peak at 612 nm disappears and new peaks at 615 and 623 nm appear. This spectrum is consistent with spectra of monoclinic nanoparticles measured previously.[13−15] In general, the emission bands are broadened and the fine structure is obscured in the nanoparticles. This is particularly clear in the samples prepared at 600, 700, and 900 °C. This broadening has been attributed to inhomogeneous broadening due to a disordering of the crystal phase, possibly induced by the increase of surface/volume ratio with decreasing size.[12−16] This broadening is less pronounced in the sample prepared at 140 °C than in the samples formed at 600, 700, and 900 °C.

The relative luminescence efficiencies of the different samples may be obtained from the photoluminescence spectra in Figure 7 due to the fact that the concentration of Eu_2O_3 is the same in all samples. The luminescence efficiency increases in the order Eu_2O_3/MCM mixture ~ 600 °C < 700 °C < 900 °C < 140 °C.

Figure 8 displays the decay curves of the $^5D_0 \rightarrow {}^7F_2$ emission at 612 nm for the Eu_2O_3/MCM-41 mixture, samples prepared by heat treatment at 140, 600, 700, and 900 °C, and bulk Eu_2O_3 powder after excitation at 525 nm. A sample made from the mixture of MCM-41 and the bulk powder shows a response identical with that of the bulk powder alone. Lifetimes recorded at both 618 and 623 nm show nearly identical characteristics. The inset in Figure 8 displays an expanded short-time region (<1 μs) of the 600 °C sample and the bulk powder. As can be observed, there is a significant fast (<15 ns) component to the lifetimes. The nanoparticle/MCM-41 samples all show that this component is a significant contribution to the luminescence, whereas in bulk Eu_2O_3 powder this component is significantly diminished. Figure 9 depicts this short-time component measured with picosecond time resolution for the 140, 600, 700, and 900 °C heat-treated samples and a Eu_2O_3 powder/MCM-41 mixture. In general, the lifetimes in this time regime for each sample are characterized by multiexponential decay dynamics with very short lifetimes in the 100 ps range followed by a longer, ~5 ns decay. It is difficult to accurately define decay lifetimes and associate them with a particular species. However, there are some very important conclusions we may obtain from these measurements. First, all samples formed with MCM-41 show the pronounced, short lifetimes. Second, the short lifetimes are similar in all samples. The decays are fastest in the 140 °C sample (3 nm size) and proceed in the order 600 °C (5 nm) > 700 °C (7 nm). The 900 °C (4 and 10 nm) sample lifetime decay is usually between the 600 and 700 °C sample decays.

The microsecond to millisecond time scale lifetimes are all multiexponential. These decays require three exponentials to adequately fit the data in this region. The results of the fitting are summarized in Table 1. It is clear from both the data and Table 1 that the lifetime of the slowest component increases in the order bulk < 140 °C < 600 °C < 700 °C < 900 °C.

Time-resolved emission spectra following excitation at 525 nm were recorded for all samples, and the results are shown in Figure 10. The gate width was set at 1 μs for all spectra. The 600, 700, and 900 °C samples all show a significant sharpening of the peak at 612 nm initially, followed by an evolution to a significantly broader spectrum. In these samples, the sharp spectrum is associated with the shortest microsecond lifetime. In the case of the 140 °C sample, the initial spectrum is not significantly sharper than a continuous-wave spectrum shown in Figure 7; however, the spectrum does broaden significantly during the final decay lifetime. The final, broadened spectra are similar in all the nanoparticle samples. In contrast, time-resolved spectra of the bulk powder show little variation over the same time range.

4. Discussion

4.1. Structure. An increasing interest in the study of guest−host composite materials[27,28] has heightened research in well-defined periodic microporous structures such as zeolites and MCM-41. These compounds are particularly attractive host materials due to their high ultraviolet transparency and are relatively inexpensive to prepare.[29] MCM-41 is a mesoporous silicate with straight, hexagonal channels and represents an interesting host material. Numerous research efforts have been reported on the encapsulation and characterization of organic compounds,[30] polymers,[31] and metal and semiconductor clusters[32,33] in MCM-41. It has been reported that nanoclusters can be encapsulated into MCM-41 at temperatures higher than 70

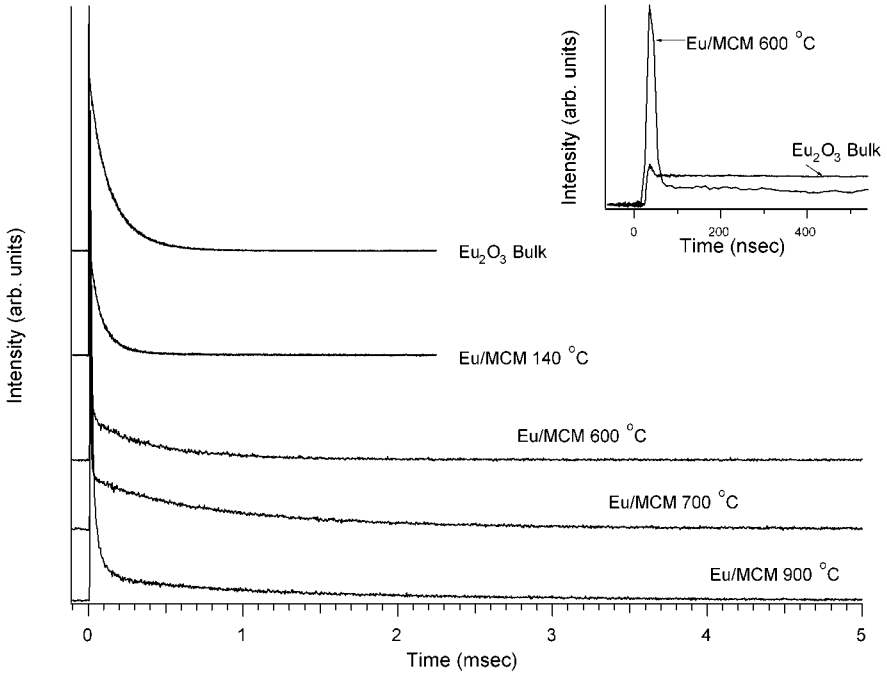

Figure 8. Lifetime decay curves of the 5D0 → 7F2 emission following excitation at 525 nm of Eu_2O_3 bulk powder, an Eu_2O_3/MCM-41 mixture, and the samples prepared by heat treatment at 140, 600, 700, and 900 °C. The inset shows an expanded view of the short-time (<1 μs) time regime for the bulk powder and the sample prepared at 600 °C.

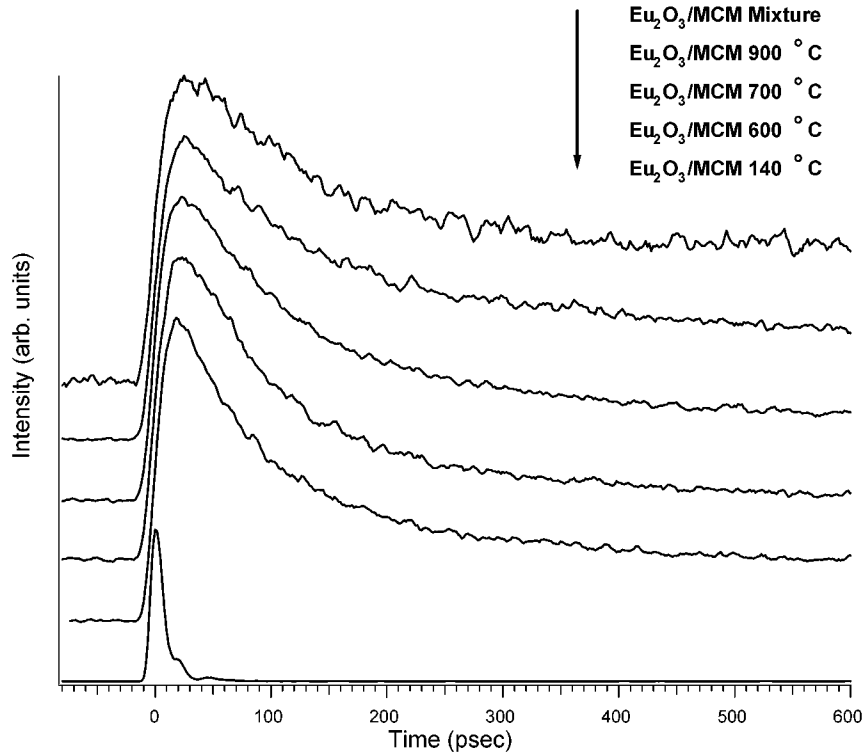

Figure 9. Picosecond lifetime decays following excitation at 400 nm of a Eu_2O_3 bulk powder/MCM-41 mixture, and samples prepared by heat treatment at 140, 600, 700, and 900 °C. The bottom trace shows the instrument response measured to be 14 ps fwhm.

°C.[23] The nanoparticles formed at 140 °C are similar in size to the pore diameter of MCM-41. Therefore, it is likely that Eu_2O_3 nanoparticles are formed within the channels of MCM-41 at 140 °C. Monoclinic Eu_2O_3 is usually stable only at high temperature and pressure.[26] The appearance of monoclinic-phase Eu_2O_3 formed at such low temperatures and pressure in air may provide a new, efficient, and low-cost method for making pure monoclinic Eu_2O_3. Previous studies have produced similar monoclinic Eu_2O_3 nanoparticles between 4 and 18 nm; however, the smallest particles are thought to return to a cubic and/or disordered phase.[12,15]

The presence of the denser, high-pressure monoclinic-phase Eu_2O_3 at ambient conditions is probably a result of the increased hydrostatic pressure resulting from the small size of the nanoparticles due to the Gibbs−Thomson effect[34] and the additional hydrostatic pressure from the walls of MCM-41 when the particles are squeezed into the channels. According to the Gibbs−Thomson effect,[34] an additional hydrostatic pressure

TABLE 1: Luminescence Decays of Eu_2O_3 Nanoparticles

Eu_2O_3 samples	lifetime (μs, 610 nm)	size (nm)
bulk (monoclinic)[a]	12 ± 2, 61 ± 6	
bulk (cubic)[a]	38 ± 2, 183 ± 9	
bulk powder	80, 170	
140 °C	15, 63, 195	3
600 °C	2, 287, 685	5
700 °C	2, 455, 1200	7
900 °C	6, 62, 1300	4, 10

[a] Reference 14.

(Δp) can result from the surface curvature of the nanometer-sized particles. The pressure increases with decreasing size (D): $\Delta p = 4\gamma/D$, where γ is the surface energy.[34] Assuming γ to be 1500 mJ m^{-2}, a typical value of surface energy for ceramics,[35] the hydrostatic pressure for a 3.5 nm-sized Eu_2O_3 particle is estimated to be around 3.4 GPa. Investigation at high pressure has demonstrated that at 5.4 GPa the cubic Eu_2O_3 phase begins to convert to the monoclinic phase; however, the complete conversion of the cubic phase to the monoclinic phase does not occur until 13.9 GPa.[35] This indicates that the hydrostatic pressure resulting from the size effect alone is not large enough to convert the cubic phase to the monoclinic phase. The additional hydrostatic pressure may come from the walls of MCM-41. The nanoparticles encapsulated into the channels at 140 °C may suffer an additional hydrostatic pressure from the walls because the channel size decreases as the samples prepared at high temperature cool to room temperature. The combined effects may be high enough to stabilize the monoclinic phase of Eu_2O_3. Therefore, the Eu_2O_3 nanoparticles that are contained within the MCM-41 channels show the monoclinic structure.

4.2. Luminescence and Dynamics. From the decay lifetimes it is clear that there are two distinct time regimes in each sample, a fast (<10 ns) decay and a slower (microsecond to millisecond) component. The fast component is present in all the samples, although it is significantly reduced in intensity in the bulk powder. The fast component is also very similar in time scale in all the samples and is slightly shorter in the smaller nanoparticles relative to the larger ones. Lifetime decays from surface states are generally very fast, on the nanosecond, picosecond, or femtosecond time scale.[36] The fact that this component is present at a reduced amount in the bulk powder and that it becomes faster with decreasing size implies that it arises from surface and defect states. Previous results from Eu_2O_3[14−16] and Eu^{3+}-doped Y_2O_3[14] nanoparticle systems have not found a significant influence from surface states, however. Because this component becomes enhanced in nanoparticles formed in MCM-41, it is also possible that energy transfer to the MCM-41 matrix also serves to significantly shorten the lifetime in this regime. The energy gap of MCM-41 is 9.0 eV;[37] therefore, it is improbable that energy may be transferred from Eu^{3+} to the MCM-41 host directly. However, energy transfer from Eu^{3+} to defect states in the MCM-41 is possible, as MCM-41 has several defect states that lie within the band gap.[37] For example, the nonbridging oxygen hole center is known to have an absorption at 1.9 eV,[37] which overlaps effectively with the emission spectrum of Eu^{3+} as shown in Figure 7. In fact, given that the samples prepared in MCM-41 show such a large picosecond to nanosecond component, it is possible that this pathway is the dominant energy dissipation pathway for Eu ions on or near the surface.

The longer time regime is characterized by multiexponential behavior that may be fit by three time constants (Table 1). The 140 °C sample shows two time constants that are nearly identical with those measured for bulk monoclinic Eu_2O_3.[14] The 140 °C sample also shows a longer, almost 200 μs decay not observed in the bulk samples or pure Eu_2O_3 nanoparticles.[14,15] Emission spectra taken during this longer lifetime show only a broad featureless peak centered at 615 nm. The 600 and 700 °C samples show an extremely fast decay of 2 μs and then two slower decays, which are longer in the 700 °C sample relative to the 600 °C. Time-resolved spectra taken during the initial fast decay reveal a sharp feature at 612 nm, whereas spectra taken during the longer decays show only the broad spectrum. The 900 °C samples show a short time constant, similar to the other 600 and 700 °C samples, and then an intermediate time constant consistent with the bulk monoclinic and 140 °C samples. Time-resolved spectra taken at the earliest delays show a peak at 612 nm from the cubic phase and a peak at about 614 nm from the monoclinic phase. This is consistent with the results from the XRD data that show both cubic and monoclinic regions within this sample. In addition there is an extremely long 1.3 ms decay. Spectra obtained during the longer lifetimes show only the broad spectra, similar to the other samples.

The narrow, short-time spectra present in the 600, 700, and 900 °C samples are likely from a narrow distribution of sites with a cubic Eu_2O_3 lattice. Analogously, in the 140 °C sample, the emission is derived primarily from a narrow distribution of monoclinic sites. These sites may represent regions within the nanoparticle with near bulk crystalline structure, likely in the core of the particles. The longer time spectra are consistent with Eu ions in a variety of sites. Previously, broadened nanoparticle spectra have been interpreted in terms of disordered phases, possibly involving surface states.[13,15] It seems unlikely that surface states have any influence on time scales this long; however, regions within the sample that are more disordered may exist and give rise to broad spectra and longer lifetimes. Previous results have only shown this disordering in smaller particles, however.[12−16] Therefore, it is possible that the presence of MCM-41 increases the disorder of the phases from those regions near the walls.

Perhaps the most surprising result is that the longest-time lifetime component increases in the order bulk < 140 °C < 600 °C < 700 °C < 900 °C. This concurrently represents an increase in the lifetime with particle size. Water complexed with Eu^{3+} is known to shorten the lifetime considerably due to fast energy transfer from the Eu^{3+} ion to the overtones of the OH stretching modes of water.[38,39] If water is present in the samples, then one would expect that samples formed at higher temperatures would contain significantly less water adsorbed to the MCM-41. Identical lifetime measurements were performed on samples that were dehydrated for 1 week at 120 °C, and no noticeable difference in the lifetimes was observed. Therefore, adsorbed water is unlikely to be the cause of the dispersion in the lifetimes.

MCM-41 is also known to have surface Si−OH groups that could shorten the lifetime, similar to the effects of water. While these groups may have an influence on the shorter time scales, i.e., they may be the source of the energy transfer observed on nanosecond or shorter time scales, they do not likely influence the longer time scale dynamics. Recent results from Eu^{3+}−Y_2O_3 nanoparticles in porous silica and MCM-41 show no dramatic shortening of the lifetimes due to the Si−OH groups.[40] In addition, the microsecond lifetimes measured here correlate well with those measured in bulk monoclinic and cubic samples where there is necessarily no influence from such moieties.[14,15]

In addition to the lengthening of the longest lifetime with formation temperature or size, the luminescence efficiency

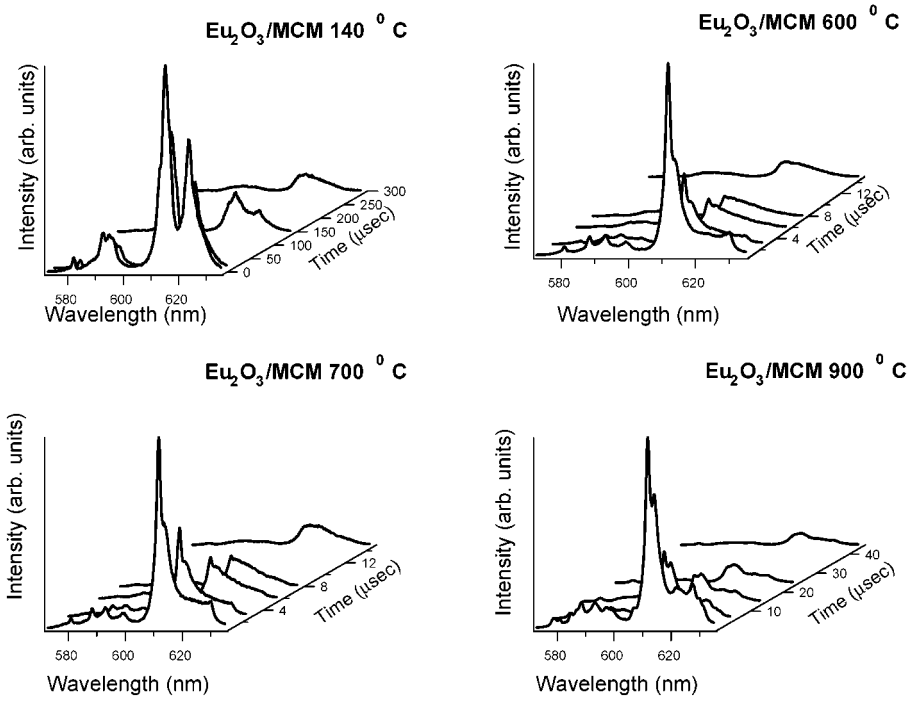

Figure 10. Time-resolved emission luminescence spectra of a Eu_2O_3 powder/MCM-41 mixture and the samples prepared by heat treatment at 140, 600, 700, and 900 °C. The gate width is 1 μs for all spectra and the excitation wavelength is 525 nm.

increases in the order 600 °C < 700 °C < 900 °C < 140 °C. The quantum efficiency (QE) of an emitter is related to the natural radiative rate k_r and the nonradiative rate k_{nr} by

$$\mathrm{QE} \sim k_r/(k_r + k_{nr})$$

The measured luminescence lifetime τ is given by

$$\tau = 1/(k_r + k_{nr})$$

From these equations, it is clear that an increase in the radiative rate will both decrease the measured lifetime and increase the quantum efficiency. An increase in the nonradiative rate will decrease the measured lifetime but will decrease the quantum efficiency as well.

The prospect of modifying the radiative lifetime and thereby enhancing the emission efficiency of phosphors is an attractive goal with a variety of potential applications to lasers, displays, and optical communications. Several means may be used to modify the radiative lifetime and emission efficiency of an emitter. These include altering the local environment of the luminescence center by putting it in different hosts, in different sites,[41] by changing the local electric field of the center by putting it in a microcavity,[42] by putting the emitter between two metal plates,[43] and by putting the sample in a medium with a high dielectric constant.[44] Modifying by quantum size confinement is a novel way under much attention.

Previous results from Y_2O_3:Eu^{3+} nanoparticles have shown that the radiative lifetime of the $^5D_0$ transition of Eu^{3+} increases by about a factor of 4 relative to micrometer-sized powder.[41] This has been attributed to changes in the local index of refraction of the nanoparticles inside the host.[41,45] A "filling factor" that describes the fraction of space occupied by the nanoparticles in the host cavity is used to calculate the effective index of refraction in the cavity.[41] The Eu_2O_3 nanoparticles formed within the MCM-41 channels may experience this effect; however, differences in the filling factor alone cannot explain the dramatic increases in lifetime observed in the larger nanoparticles. It is also possible that there is a change in the radiative rate with size due to quantum confinement. However, results from pure Eu_2O_3 nanoparticles of similar sizes as those studied here do not show dramatic or even systematic lifetime dependences on size.[12,15] Therefore, differences in the radiative transition rate are not likely causing the dramatic changes in lifetime observed here.

In addition to radiative rate modification, there are many sources of nonradiative quenching including electron−phonon coupling, concentration quenching, and quenching via surface or defect states. As mentioned earlier, quenching by surface states often results in extremely short lifetimes similar to the subnanosecond ones measured. Previous results on Eu_2O_3 and Eu^{3+}-doped Y_2O_3 nanoparticles show that electron−phonon coupling increases with decreasing particle size.[20] Eu^{3+} excited-state lifetimes were observed to be up to 2 orders of magnitude shorter in nanoparticles relative to the bulk.[46] While the trend to shorter lifetimes with decreasing particle size is consistent with this picture, we note that the lifetimes reported here are all longer than the bulk lifetimes, in contrast to the results from ref 42. Still, changes in the electron−phonon coupling as a function of the particle size cannot be ruled out.

Eu-doped samples are known to suffer concentration quenching as a result of ion−ion interactions that require relatively close proximity. It is likely that the shortened lifetimes of bulk samples of Eu_2O_3 are the result of such quenching, as doping Eu^{3+} at low concentrations into Y_2O_3 or other host materials returns the lifetime to a value close to the natural radiative rate.[14,16,21,41,47] Concentration quenching may be decreased in the samples formed at higher temperatures. This may be a result of Eu migration to the walls or even inside the MCM-41 matrix. Higher-temperature formation may permit Eu ions to migrate farther and therefore become more isolated from each other. We note that Eu nanoparticles doped in alumina have a lifetime of 1.5 ms, while those that are simply deposited on the alumina have a 340 μs lifetime.[21] These results have been interpreted in terms of the reduced concentration quenching experienced by

the Eu ions doped in the alumina.[21] This behavior is extremely similar to what is reported here. The broad spectrum may then simply reflect the large number of sites occupied by the Eu ions on or inside the MCM-41. In essence, this would represent a disordering of the pure phases present in the interior of the nanoparticles.

Therefore, it is likely that a decrease in either electron−phonon coupling or concentration quenching is causing the lengthening of the lifetimes in these samples. The increase in luminescence efficiency from the 600 °C sample to the 900 °C sample is certainly consistent with such a picture. In the sample prepared at 900 °C, some new or disordered phase is formed in the MCM-41. This different phase might also affect the luminescence behavior of Eu^{3+} in that sample.

The increase of the luminescence efficiency of the 140 °C sample may reflect a decrease in the nonradiative rate due to the different crystal structure or an increase in the radiative rate, due to either a change in symmetry or the effect of the local dielectric constant within the cavity.[41,45] The enhancement of the luminescence efficiency indicates that the nanophase materials formed at 140 °C may be efficient luminescence materials with potential applications in lighting and displays.

5. Summary

Eu_2O_3 nanoparticles of monoclinic structure are formed inside channels of MCM-41 at 140 °C. Upon heat treatment at 600 or 700 °C, the Eu_2O_3 migrates to form nanoparticles of cubic structure outside the channels. After heating at 900 °C, some of the cubic Eu_2O_3 changes to monoclinic Eu_2O_3, the MCM-41 structure breaks down, and a different phase is formed. As a consequence, the luminescence spectrum of Eu^{3+} in the sample prepared at 140 °C is different from the bulk cubic Eu_2O_3 and other Eu_2O_3/MCM-41 samples prepared at 600, 700, and 900 °C. One obvious feature is the $^5D_0 \rightarrow {}^7F_2$ emission profiles and lifetimes. The luminescence lifetimes from all the samples show very short lifetimes associated with surface states or energy transfer as well as longer lifetimes, which increase in the order bulk powder < 600 °C < 700 °C < 900 °C. This dramatic change in lifetime is attributed to a reduction in concentration quenching as Eu ions become isolated, either within or adsorbed on the MCM-41 matrix. The sample prepared at 140 °C shows a noticeably stronger luminescence efficiency that may be the result of a decreased nonradiative transition rate.

Acknowledgment. W.C. thanks Nomadics, Inc., the National Science Foundation (NSF), and the National Institute of Health (NIH) for financial support. Y.H. thanks the Natural Sciences and Engineering Research Council of Canada for financial support. J.-O.M. and J.-O.B. thank the Swedish Natural Science Research Council and the Foundation for Strategic Research of Sweden for financial support. Part of the research described in this paper was performed at the W. R. Wiley Environmental Molecular Sciences Laboratory, a national scientific user facility sponsored by the Department of Energy's Office of Biological and Environmental Research and located at the Pacific Northwest National Laboratory (PNNL). PNNL is operated by Battelle for the U.S. Department of Energy under Contract DE-AC06-76RLO1830.

References and Notes

(1) Weber, M. J. In *Handbook on the Physics and Chemistry of Rare Earths*; Gschneider, K. A., Jr., Eyring, L., Eds.; North-Holland: New York, 1979; Vol. 4, Chapt. 35, pp 275−315.
(2) Rosynek, M. P. *Catal. Rev. Sci. Eng.* **1977**, *16*, 111.
(3) Itoh, S.; Toki, H.; Sato, Y.; Morimoto, K.; Kishino, T. *J. Electrochem. Soc.* **1991**, *138*, 1509.
(4) Blasse, G. In *Luminescence of Inorganic Solids*; Di Bartolo, Ed.; Plenum Press: New York and London, 1977; pp 457−494.
(5) Blasse, G. *Struct. Bonding* **1976**, *26*, 43.
(6) Sheng, K. C.; Korenowski, G. M. *J. Phys. Chem.* **1988**, *92*, 50.
(7) Brittain, H. G.; Pery, D. L. *J. Catal.* **1982**, *77*, 94.
(8) Bhargava, R. N. *J. Lumin.* **1996**, *70*, 85.
(9) Chen, W.; Sammynaiken, R.; Huang, Y. *J. Appl. Phys.* **2000**, *88*, 5188.
(10) Chen, W.; Sammynaiken, R.; Huang, Y.; Malm, J.-O.; Wallenberg, R.; Bovin, J.-O.; Zwiller, V.; Kotov, N. A. *J. Appl. Phys.* **2001**, *89*, 1120.
(11) Chen, W.; Malm, J.-O.; Zwiller, V.; Huang, Y.; Liu, S. M.; Wallenberg, R.; Bovin, J.-O.; Samuelson, L. *Phys. Rev. B* **2000**, *61*, 11021.
(12) Tissue, B. M. *Chem. Mater.* **1998**, *10*, 2837.
(13) Eilers, H.; Tissue, B. M. *Chem. Phys. Lett.* **1996**, *251*, 74.
(14) Bihari, B.; Eilers, H.; Tissue, B. M. *J. Lumin.* **1997**, *75*, 1.
(15) Tissue, B. M.; Bihari, B. *J. Fluoresc.* **1998**, *8*, 289.
(16) Williams, D. K.; Yuan, H.; Tissue, B. M. *J. Lumin.* **1999**, *83*/*84*, 297.
(17) Patra, A.; Sominska, E.; Ramesh, S.; Koltypin, Y.; Zhong, Z.; Minti, H.; Reisfeld, R.; Gedanken, A. *J. Phys. Chem. B* **1999**, *103*, 3361.
(18) Wakefield, G.; Keron, H. A.; Dobson, P. J.; Hutchison, J. H. *J. Colloid Interface Sci.* **1999**, *215*, 179.
(19) Meltzer, R. S.; Hong, K. S. *Phys. Rev. B* **2000**, *61*, 3396.
(20) Hong, K. S.; Meltzer, R. S.; Bihari, B.; Williams, D. K.; Tissue, B. M. *J. Lumin.* **1998**, *76*/*77*, 234.
(21) Gedanken, A.; Reisfeld, R.; Sominski, L.; Zhong, Z.; Koltypin, Y.; Panszer, G.; Gaft, M.; Minti, H. *Appl. Phys. Lett.* **2000**, *77*, 945.
(22) Beck, J. S.; Vartuli, J. C.; Roth, W. J.; Leonowicz, M. E.; Kresge, C. T.; Schmitt, K. D.; Chu, C. T.-W.; Olson, D. H.; Sheppard, E. W.; McCullen, S. B.; Higgens, J. B.; Schlenker, J. L. *J. Am. Chem. Soc.* **1992**, *114*, 10834.
(23) Kowalchuk, C.; Corrigan, J.; Huang, Y. *Chem. Commun.* **2000**, 1811.
(24) Klug, H. P.; Alexander, L. E. *X-ray Diffraction Procedure*, 2nd ed.; Wiley: New York, 1974.
(25) Carnell, W. T. *Handbook on the Physics and Chemistry of Rare Earths*; North-Holland Publishing Company: Amsterdam, 1979; Vol. 3, p 171.
(26) Chen, G.; Stump, N. A.; Haire, R. G.; Peterson, J. R. *J. Alloys Compounds* **1992**, *181*, 503.
(27) Moller, K.; Bein, T. *Chem. Mater.* **1998**, *10*, 2950.
(28) Ozin, G. A. *Adv. Mater.* **1992**, *4*, 612.
(29) Engel, S.; Kynast, U.; Unger, K. K.; Schuth, F. *Stud. Sci. Catal.* **1994**, *84*, 477.
(30) Wu, C.; Bein, T. *Chem. Mater.* **1994**, *6*, 1109.
(31) MacLachlane, M. J.; Aroca, P.; Coombs, N.; Manners, I.; Ozin, G. A. *Adv. Mater.* **1998**, *10*, 144.
(32) Sasaki, M.; Osada, M.; Sugimoto, N.; Inagaki, S.; Fukushima, Y.; Fukuoka, A.; Ichikawa, M. *Microporous Mesoporous Mater.* **1998**, *21*, 597.
(33) Leon, R.; Magolese, D.; Stucky, G.; Petroff, P. M. *Phys. Rev. B* **1995**, *52*, 2285.
(34) Porter, D. A.; Eastering, K. E. *Phase Transformations in Metals and Alloys*; Chapman and Hall: London, 1991.
(35) Skandan, G.; Foster, C. M.; Ali, M. N.; Parker, J. C.; Hahn, H. *Nanostruct. Mater.* **1992**, *1*, 313.
(36) Lefebvre, P.; Mathieu, H.; Allegre, J.; Richard, T.; Combettes-Roos, A.; Pauthe, M.; Granier, W. *Semicond. Sci. Technol.* **1997**, *12*, 958.
(37) Gimon-Kinsel, M. E.; Groothuis, K.; Balkus, K. J., Jr. *Microporous Mesoporous Mater.* **1998**, *20*, 67.
(38) Hazenkamp, M. F.; van Veen, A. M. H.; Feiken, N.; Blasse, G. *J. Chem. Soc., Faraday Trans.* **1992**, *88*, 141.
(39) Bartlett, J.; Cooney, R. P.; Kydd, R. A. *J. Catal.* **1988**, *114*, 58.
(40) Schmechel, R.; Kennedy, M.; von Seggern, H.; Winkler, H.; Kolbe, M.; Fischer, R. A.; Xaomao, L.; Benker, A.; Winterer, M.; Hahn, H. *J. Appl. Phys.* **2001**, *89*, 1679.
(41) Meltzer, R. S.; Feofilov, S. P.; Tissue, B.; Yuan, H. B. *Phys. Rev. B* **1999**, *60*, R14012.
(42) Chang, R. K.; Campillo, A. J. *Optical Processes in Microcavities*; World Scientific: Singapore, 1996.
(43) Kummerlen, J.; Leitner, A.; Brunner, H.; Aussenegg, F. R.; Wokaun, A. *Mol. Phys.* **1993**, *80*, 1031.
(44) Okamoto, K.; Nasu, Y.; Hamakawa, Y. *IEEE Trans. Electron Devices* **1981**, *28*, 698.
(45) Meltzer, R. S.; Yen, W. M.; Zheng, H.; Feofilov, S. P.; Dejneka, M. J.; Tissue, B. M.; Yuan, H. B. *J. Lumin.* **2001**, *94*/*95*, 217.
(46) Yang, H.; Hong, K. S.; Feofilov, S. P.; Tissue, B. M.; Meltzer, R. S.; Dennis, W. M. *J. Lumin.* **1999**, *83*/*84*, 139.
(47) Williams, D. K.; Bihari, B.; Tissue, B. M. *J. Phys. Chem. B* **1998**, *102*, 916.